CBPF - CENTRO BRASILEIRO DE PESQUISAS FÍSICAS

Rio de Janeiro

Notas de Física

SW 9620

Fissility of Bi, Pb, Au, Pt, W, Ta, V, and Ti Nuclei Measured with 100-MeV Compton Back-Scattered Photons

M.L. Terranova, O.A.P. Tavares, G.Ya. Kezerashvili, V.A. Kiselev,

A.M. Milov, N. Yu. Muchnoi, A.I. Naumenkov, V.V. Petrov,

I. Ya. Protopopov, E.A. Simonov, E. de Paiva and E.L. Moreira

FISSILITY of Bi, Pb, Au, Pt, W, Ta, V, and Ti NUCLEI MEASURED WITH 100-MeV COMPTON BACK-SCATTERED PHOTONS

M.L.Terranova and O.A.P.Tavares[*]
Dipartimento di Scienze e Tecnologie Chimiche, Universita' di Roma "Tor Vergata", and Istituto Nazionale di Fisica Nucleare- INFN, Sezione di Roma 2, 00133 Roma, Italy

G.Ya.Kezerashvili, V.A.Kiselev, A.M.Milov, N.Yu. Muchnoi, A.I.Naumenkov, V.V.Petrov, I.Ya. Protopopov, and E.A.Simonov
Budker Institute of Nuclear Physics, Academy of Sciences of Russia ,Siberian Division, 630090 Novosibirsk, Russia

E de Paiva[**] and E.L.Moreira
Conselho Nacional de Desenvolvimento Cientifico e Tecnologico-CNPq, Centro Brasileiro de Pesquisas Fisicas-CBPF, 22290-180 Rio de Janeiro, RJ, Brazil

Abstract

Photofission cross sections of ^{209}Bi, ^{nat}Pb, ^{197}Au, ^{nat}Pt, ^{nat}W, ^{181}Ta, ^{51}V, and ^{nat}Ti nuclei have been measured at an incident photon energy of 100 MeV using monochromatic photons produced by Compton backscattering at the ROKK-1M facility (BINP,Novosibirsk) . Detection of fission fragments has been performed by means of Makrofol track-etch detectors in close contact with metallic foils of the target elements. The values of fissility at 100 MeV deduced for the targets under investigation are found to range between 10^{-4} and 10^{-2} . The present results show consistency with the fissility trends calculated for 69- and 600-MeV monoenergetic photons using a formalism based on the current two-step model for intermediate-energy photofission reactions .

PACS: 25.85.-w, 25.85.Jg

----

[*] Permanent address:Conselho Nacional de Desenvolvimento Científico e Tecnológico-CNPq,Centro Brasileiro de Pesquisas Fisicas-CBPF, 22290-180 Rio de Janeiro-RJ, Brasil
[**] Fellow, Brazilian CNPq, contract nr. 840003/92-7.

1.Introduction

The experimental investigation of nuclear fission induced in pre-actinide nuclei by intermediate-energy photons has revealed interesting features .Pre-actinide nuclei do not exhibit at low incident energies (k $\lesssim$ 30 MeV) the resonance pattern characteristic of the fission cross section of actinide nuclei. For nuclei of mass number A < 210 the trends of the photofission cross section σ_f, and of the fissility ,f (ratio of fission cross section to total nuclear photoabsoption cross section), show conversely an increase of several orders of magnitude from fission threshold ($\sim$20-30 MeV) up to about 200 MeV.

Most of the investigations on photofission of pre-actinides were carried out using bremsstrahlung radiation as a source of real photons [1-7]. In some instances photofission cross sections for pre-actinide and intermediate-mass nuclei were obtained by unfolding the electrofission yields with a virtual photon spectrum [8-11]. In recent years the development of new techniques allowed to use monochromatic photon beams and/or tagged photons [12-19] and to obtain more reliable photofission cross section data at energies k$\lesssim$ 140 MeV [20-27].

We have concentrated our interest on the study of photofission of pre-actinides and intermediate-mass nuclei in the quasi- deuteron region of photonuclear interaction (30$\lesssim$ k $\lesssim$ 140 MeV). Accordingly, we have planned a series of photofission experiments taking advantage of the monochromatic photon beams of the ROKK-1M facility (BINP, Novosibirsk, Russia) and of a detection technique which uses solid-state fission track detectors in contact with thick targets [28] for evaluation of low fission yields .

The current research represents an extension towards higher energies of that performed by some of us by using monochromatic photons of 69 MeV (LADON facility at the Frascati National Laboratories) [25 -27]. Following the same approach, the present paper reports fissility data collected at a fixed energy for various target nuclei. Here, photofission has been induced in ^{209}Bi, ^{nat}Pb, ^{197}Au, ^{nat}Pt, ^{nat}W, ^{181}Ta, ^{51}V and ^{nat}Ti by monochromatic photon beams of 100 MeV. The dependence of fissility upon parameter Z^2/A for pre-actinide and intermediate-mass nuclei is discussed on the basis of the present results and of the data obtained in other laboratories.

2. Experimental

The stacks containing the various target materials in close contact with makrofol fission-track detectors were exposed to the monochromatic photon beams produced at the ROKK-1M facility by Compton back-scattering of laser light against high-energy electrons (1.8 GeV) circulating in the VEPP-4M storage ring. The experimental set-up is shown in figure1. The Compton scattering between a relativistic electron beam and laser light enhancesthe energy of the laser photons in the head-on collision. Doubled base harmonic of Q-switched Nd:Yag laser (omega = 2.34 eV) are used. The laser beam focused on the interaction point is injected into the vacuum chamber of the VEPP-4M collider beside the bending magnet. The γ-flux get out of the vacuum chamber through the last mirror M2, passing thereafter the collimator C (a rectangular 4x4 mm hole in 100 mm lead shield) and the cleaning magnet CM placed at 18 m from the interaction point. Due to the correlation between energy and emission angle of γ-quanta, the collimator adsorbes the low-energetic part of the Compton spectrum and decreases the flux of the bremsstrahlung γ-quanta produced in the collider straight region. The γ-beam profile after collimation is measured by a space-sensitive detector consisting of a two-coordinate multiwire proportional chambers with 2 mm lead convertor. The energy spectrum is taken by a NaI(Tl) total photo-absorption calorimeter . The scintillation counter SC placed before the NaI(Tl) detector is used as a trigger for the charged particles of the γ-beam. Coincidences between the signals coming from calorimeter, scintillation counter, and laser pulses are used to define the contributions of Compton, bremsstrahlung and charged components in the flux. A detailed description of the ROKK-1M facility can be found in Ref. [29].

In figure 2 is reported a typical spectrum of the γ-beam, obtained by the following procedure. The NaI (Tl) calorimeter was calibrated in the whole range of γ-quanta energy by using the KEDR detector tagging system [30] that provides a resolution of the electron beam energy better than 0.1% . The response function of the of the NaI(Tl) calorimeter was measured. The resolution of the NaI(Tl) calorimeter was found to be (11÷16)% in the range of the Compton spectrum energies. The corrected γ-beam spectrum obtained by the deconvolution of the detector response function (figure 2) shows a Compton-edge of k_{max} = 109 MeV , a peak width (FWHM/k_{max}) of about 18% , and an energy threshold of 14.6 MeV. The ratio of Compton to bremsstrahlung photons , in the whole spectrum, was better than 9.0 (first run)

and 6.0 (second run).The percentage of charged particles in the total dose was less than 7% (first run) and 12% (second run). The real doses collected by each target have been evaluated taking into account the photon flux attenuation through the stacks and are listed in table 1.

Table 1 gives a description of the target and detector materials used in the experiments. Data have been collected in two runs.

After irradiations, the detector foils were processed by the usual etching procedure [26] in order to obtain legible fission fragment tracks on the detector surface for track counting by optical microscopy (table 1).Since the total area to be scanned was very large (~1440 cm^2), track identification on each detector was done by one observer (single scanning) and checked by a second one. Track loss during the optical analysis has been estimated from previous double scanning photofission experiments performed with the same methodology [25-27]. In this way, a counting efficiency of (79 ± 7)% was evaluated and throughly adopted in converting track counting into fission yields.

3.Data analysis and results

To obtain the physical quantities of interest and associated errors, the data have been treated by taking into account statistics and efficiency of track counting. We introduced also the appropriate corrections for both γ-beam attenuation through the stacks and self-absorption of fission fragments by the target materials (thin- and thick-target geometry). Accordingly, the nominal total photon doses have been corrected by using the law of exponential decrease of photon beam intensity in passing through the matter (see table 1). For the second correction it was necessary to determine the effective thickness , x ,of each target, and the average total efficiency , ε , of the detection method (etching efficiency multiplied by observation efficiency). The evaluation of the quantity x takes into account the average residual range of the full-energy median fission fragment in both target and detector materials . The value of ε has been evaluated by considering: i) the thickness of the surface layer of the detector removed by etching ; ii) the minimal etched fission track projection capable of being observed on the detector surface under given optics. All these quantities have been handled following the procedure described in details in Refs. [26] and [28], and the resulting values of x and ε for the two runs are listed in table 2. Finally, for each target element, the total number of fission events has been obtained by summing over the number of detectors

employed in the two runs.

3.1. Photofission yield

For fission experiments performed by using target materials in close contact with fission-track detectors, the fission yields are expressed by the formula

$$Y = C \times \frac{\sum_{i=1}^{2} N_{T_i}}{\sum_{i=1}^{2} Q_i \cdot n_i \cdot \varepsilon_i x_i} \quad , \tag{1}$$

where $C = M /(\rho N_o)$ is a constant for each target element, M is the atom-gram, ρ is the density and N_o is Avogadro's number. The other quantities appearing in (1) are defined and listed in tables 1 and 2. The last column in table 2 reports the values of the photofission yield for the various target nuclei. The main source of error is the statistical one (~ 20-30% for Bi, Pb, and Pt, ~ 44% for Au, W, Ta, and 50-60% for V and Ti targets). Systematic errors amount to ~ 22% for for Bi and Au, 18% for Pb, and 13% for Pt, W, Ta, V, and Ti targets.

As can be seen from inspection of table 2, the present method allowed us to measure photofission yields as low as some units of μb. This was possible in view of both the photon doses provided by the ROKK-1M facility and the large number of fission track detectors employed in the experiments.

3.2. Absolute photofission cross section

The measured photofission yield, Y, is related to the absolute photofission cross section, σ_f, through the relationship

$$Y = \int_{k_i}^{k_f} \sigma_f(k) \left(\frac{dn}{dk} \right) dk \quad , \tag{2}$$

where k_i and k_f are the limiting energy values in the photon spectrum, and $dn/dk = p(k)$ represents the fraction of photons in the energy interval dk , i.e.,

p(k) is the energy distribution normalized to one photon in the range k_i-k_f.
In order to calculate the relative contributions to the total yield due to low-
(k << k_{max}) and high-energy (k > k_{max}) photons in the spectrum, the integral
(2) is rewritten as

$$Y = \int_{k_{th}}^{k_1} \sigma_f(k)p(k)dk + \int_{k_1}^{k_2} \sigma_f(k)p(k)dk + \int_{k_2}^{k_f} \sigma_f(k)p(k)dk \quad , \qquad (3)$$

with k_{th} standing for the photofission threshold. The effective photon energy
interval k_1-k_2 contains the peak of the energy distribution and is defined in
such a way that

$$\int_{k_{th}}^{k_1} \sigma_f(k)p(k)dk + \int_{k_2}^{k_f} \sigma_f(k)p(k)dk \ll \int_{k_{th}}^{k_f} \sigma_f(k)p(k)dk \quad . \qquad (4)$$

In order to define the values of k_1 and k_2 for Bi, Pb and Au targets, we have
used in (4) the trends obtained from the measured values of σ_f [4,6,8-
10,20,22,23,25]. In view of the fact that the experimental yields are affected by
large errors, it is reasonable to admit that a 20-25% of fission events are due
to low- and high-energy photons. In this way, it was found k_1=90 MeV,
k_2=115 MeV, and the average photon energy in the measured energy
spectrum results to be $\bar{k}$ = 100 MeV. Inspection of figure 3 shows the relative
contributions to the total yield from the different photon energy regions
mentioned (bottom scale) for Bi **(a)** and Pb and Au targets **(b).** Since the
peak-shape of the spectrum is reasonably narrow in the range k_1-k_2, it follows
that $\sigma_f(\bar{k})$ = α Y . The numerical factor α turns out to be 1.37 for Bi, and
1.40 for Pb and Au. The average value of 1.39 has been used. For the other
pre-actinide target nuclei one can assume the same value for the α-factor,
because their relative contributions to the total yield are expected not to differ
significantly from those of Bi, Pb, and Au nuclei.
For nuclei of mass number A $\leq$ 100, the photofission threshold, k_{th} , can be
evaluated from the average total kinetic energy released in fission , $<E_k^t>$, and
from the Q-value for the nearly symmetric break-up of the fissioning nucleus.
One obtains k_{th} = $<E_k^t>$ - Q, where Q is a negative quantity. The
$<E_k^t>$-values have been calculated from the systematics reported in [31],
and the Q- values from the Table of Mass by Audi and Wapstra [32]. In this
way, the photofission threshold for ^{51}V and ^{nat}Ti is found to be k_{th} $\cong$ 50
MeV. Since for these two target nuclei the trend of σ_f is unknown, the best we

can do is to assume $\bar{k}$ =100 MeV valid also for these two targets , and write

$$\sigma_f(\bar{k}) = \frac{Y}{\int_{k_1}^{k_f} p(k)\,dk} \qquad , \qquad (5)$$

where $\bar{k}$ is now defined in the range k_1 - k_f. By using this procedure one obtains k_1=80 MeV and $\sigma_f(\bar{k})$ =1.39 Y. Surprisingly, the numerical factor relating $\sigma_f(\bar{k})$ to Y results to be the same as for the pre-actinide nuclei. In summary, for all the target elements studied in the present work , the absolute photofission cross sections at k=100 MeV could be obtained by multiplying the measured photofission yields by the factor 1.39. The resulting cross sections are reported in table 3 (4th column) together with data from other laboratories.

3.3. Nuclear Photofissility

Photofissility values at k=100 MeV have been deduced by calculating the ratio

$$f = \sigma_f/\sigma_a^t , \qquad (6)$$

where the total nuclear photoabsorption cross section, σ_a^t , has been evaluated according to Levinger's modified quasi-deuteron model [33]

$$\sigma_a^t(k) = L\frac{NZ}{A}\sigma_d(k)\,e^{-Dk} \qquad (7)$$

Here, $\sigma_d(k)$ stands for the total photodisintegration cross section of the free deuteron , the value of which at k=100 MeV is 73 μb [34]. L is Levinger's constant calculated by $L = 6.8 - 11.2\,A^{-2/3} + 5.7\,A^{-4/3}$ according to [35]. D is the so-called "damping " parameter given by $D = 0.72\,A^{0.81}$ MeV [36] . Finally, NZ represents the number of neutron-proton pairs of the target nucleus. The dependence of σ_a^t on mass number, calculated by equation (7) , is depicted in figure 3 (c) (top scale). The reported trend agrees rather well with

the available measured σ_a^t- values (points) from Refs.[12] and [37]. Therefore, use has been made of equation (7) to evaluate σ_a^t-values. The corresponding photofissilities for the nuclei considered in the present work have been throughly determined by equation (6). All these data are reported in table 3.

4. Discussion

The photofissility data reported in table 3 show a general trend of increasing with Z^2/A from the region of rare earth elements up to the heavier pre-actinides. This feature is better evidenced in figure 4, and it is consistent with the predictions based on the fission-evaporation competition model by Nix and Sassi [38], as well as with the detailed cascade-evaporation model by Iljinov et al. [39]. In figure 4 we chose to report, along with the present results (filled circles), literature data obtained by quasi-monochromatic photons (open symbols). A representative result for ^{nat}Tl (filled triangle) and interpolated fissility values for ^{174}Yb and ^{154}Sm obtained by virtual photons [8] are also shown in figure 4.These latter data represent the unique available information in the region of intermediate-mass nuclei. As expected it is found that, within the referred uncertainties, the set of data points obtained at k=100 MeV lies between the fissility trends calculated for monoenergetic photons of 69 MeV [25,27] (full line) and of 600 MeV [39] (dotted line). Moreover, the data appear closer to the fissility trend calculated for 69 MeV than to that for 600 MeV. This feature is consistent with the predictions of the current model for intermediate-energy photofission reactions.

As far as the ^{51}V and ^{nat}Ti targets are concerned, it is worth noticing that ,for nuclei lighter than silver, both a study of nuclear fissility throughout the periodic table [38] and Monte Carlo calculations of photon-induced reactions based on the cascade-evaporation model [39] have indicated a clear trend of fissility increasing with Z^2/A decreasing. Recently, in a study of ^{27}Al fission by 69-MeV monochromatic photons [27], such calculations have been extended towards less massive nuclei (left portion of the full line in figure 4). Although no trend of calculated fissility is at present available for incident photons of 100 MeV , the experimental values here determined for ^{51}V and ^{nat}Ti ($\sim 10^{-2}$) seem to confirm the predicted increasing of fissility for fissioning systems with $Z^2/A \lesssim 20$.

5.Conclusions

In the course of the present work, the fission of some pre-actinide nuclei (^{209}Bi, ^{nat}Pb, ^{197}Au, ^{nat}Pt, ^{nat}W, and ^{181}Ta) and of two less massive nuclei (^{51}V and ^{nat}Ti) has been investigated by using monochromatic photon beams of 100 MeV produced from Compton backscattered laser light. Photofission yields have been measured taking advantage of a method which uses makrofol fission-track detectors in close contact with thick target materials. It is to be noted that this paper reports the first experimental determination of fission yields for ^{nat}W, ^{51}V, and ^{nat}Ti targets in the quasi-deuteron region of photonuclear absorption. For the various target nuclei the absolute photofission cross sections ,σ_f, have been determined taking into account the photon spectrum .Photofissility values were subsequently deduced for each target element from the ratio σ_f / σ_a^t where σ_a^t is the total nuclear photoabsorption cross section at 100 MeV ,calculated in the framework of Levinger's modified quasi-deuteron model. The results were compared with available data obtained by incident photons of 100 MeV ,and a satisfactory agreement has been found.

Overall, the whole set of fissility data obtained in the present work shows to be consistent with the trends calculated at 69- and 600-MeV on the basis of the fission-evaporation competition model for photofission reactions, as well as with data of other pre-actinide and intermediate-mass nuclei from other laboratories. In particular, the present data for ^{51}V and ^{nat}Ti nuclei appear to follow the predicted increase of fissility with Z^2/A decreasing in the region of light complex nuclei.

Further experiments of fission induced in the same target nuclei by higher energy monochromatic photons are being carried out presently in our laboratory.

Figure Captions

Figure 1. Experimental setup of the ROKK-1M facility at the storage ring VEPP-4 (BINP, Novosibirsk, Russia): LS is the the laser source ; L1, L2 are focusing lenses ; M1, M2 are mirrors ; C is a 4mmx4mm collimator of 10 cm of lead ; CM is a cleaning magnet ; SC is a scintillation counter ; T+D are the stacks of targets and makrofol detectors ; PC is a proportional chamber with 2 mm lead converter ; NaI(Tl) is a total photoabsorption calorimeter of 10 cm x 10 cm x 40 cm for gamma-beam spectrometry and dose measurements.

Figure 2. Typical spectrum of back-scattered Compton γ-beam (normalized to one photon) taken with the NaI(Tl) calorimeter after collimation.

Figure 3. (a) Fission-yield strength, $\sigma_f(k)$ (dn/dk) , plotted against photon energy (bottom scale) for Bi targets . $\sigma_f(k)$ is the average trend from data of Refs. [6, 8, 9, 20, 22, 25] for Bi , dn/dk is the measured Compton spectrum shown in figure 2. The energy-values k_{th} , k_1, and k_2 define the various energy regions in equation (3). (b) The same for Pb and Au targets : $\sigma_f(k)$ is the average trend from data of Refs.[4 , 23] for Au, and the measured σ_f curve of Ref.[10] for Pb.
(c) Total nuclear photoabsorption cross section, σ_a^t , plotted against mass number A (top scale) for incident photons of 100 MeV. The curve has been obtained from equation (7) as explained in the text ; points represent experimental results for Ca from Ref. [37], and Sn,Ce, Ta, Pb, and U from Ref.[12].

Figure 4. Nuclear fissility plotted against parameter Z^2/A of the target nucleus. Points represent experimental data for 100- MeV incident photons: ●, ^{209}Bi, ^{nat}Pb, ^{197}Au, ^{nat}Pt, ^{nat}W, ^{181}Ta, ^{51}V and ^{nat}Ti of this work ; ◯ ^{209}Bi of Ref.[22] ; ☐ ,^{209}Bi of Ref.[21] ; ■ ^{174}Yb and ^{154}Sm of Ref.[8] ; ▲ ^{nat}Tl of Ref.[5] ; △ ^{197}Au of Ref.[23]. For comparison, two results of calculated fissility are shown: solid line, 69-MeV monoenergetic photons from Refs. [25] and [27] ; dotted line, 600-MeV monoenergetic photons from Ref.[39].
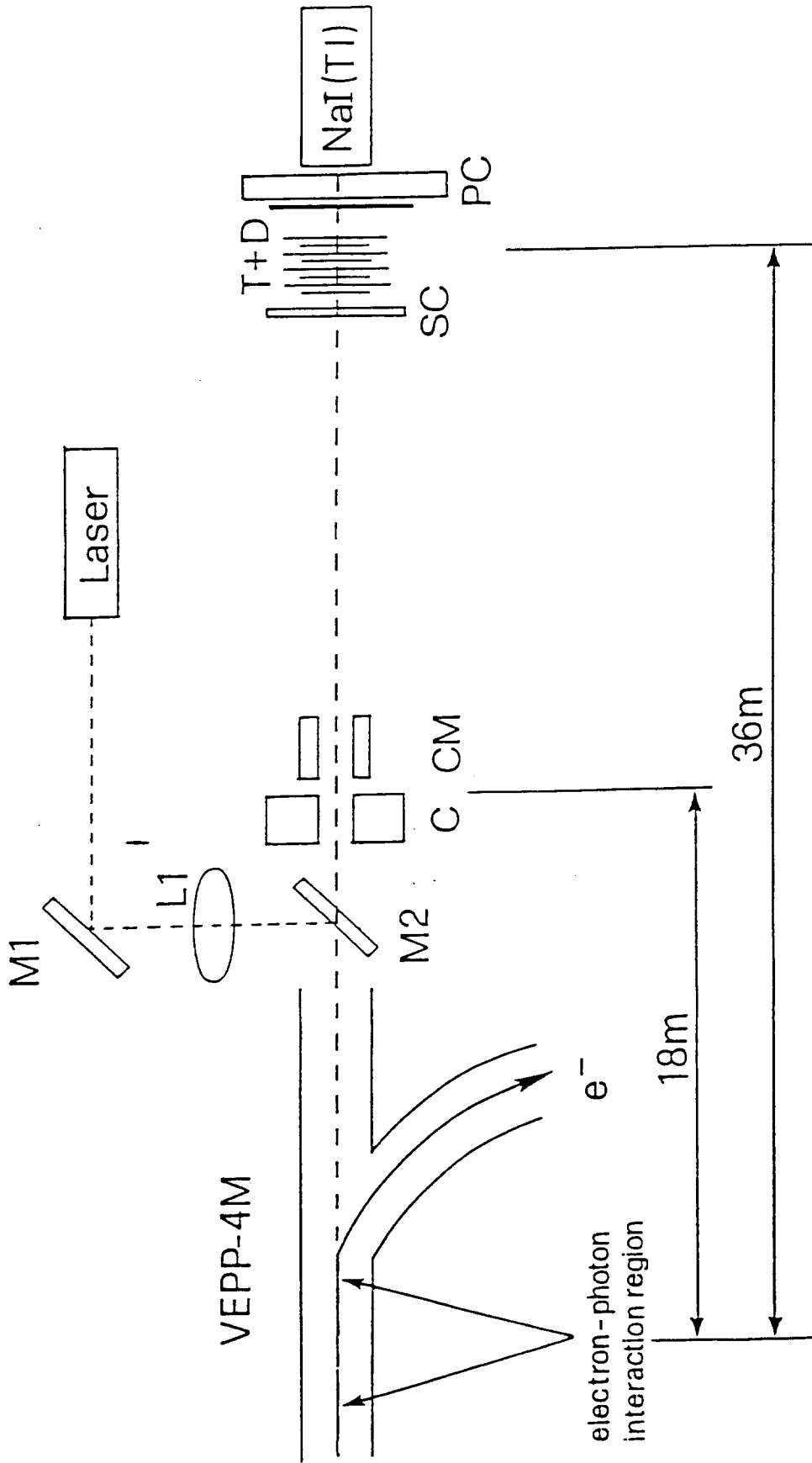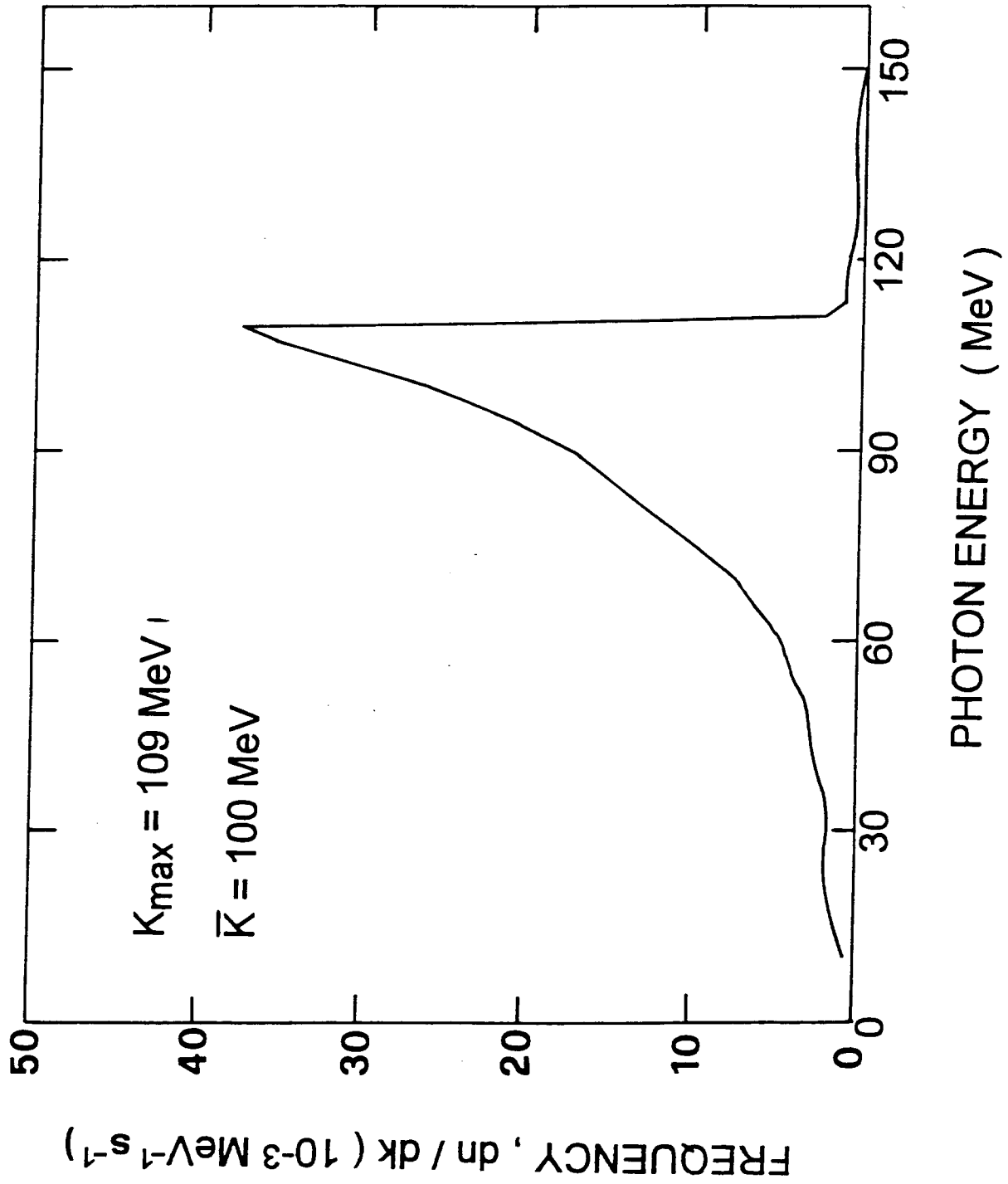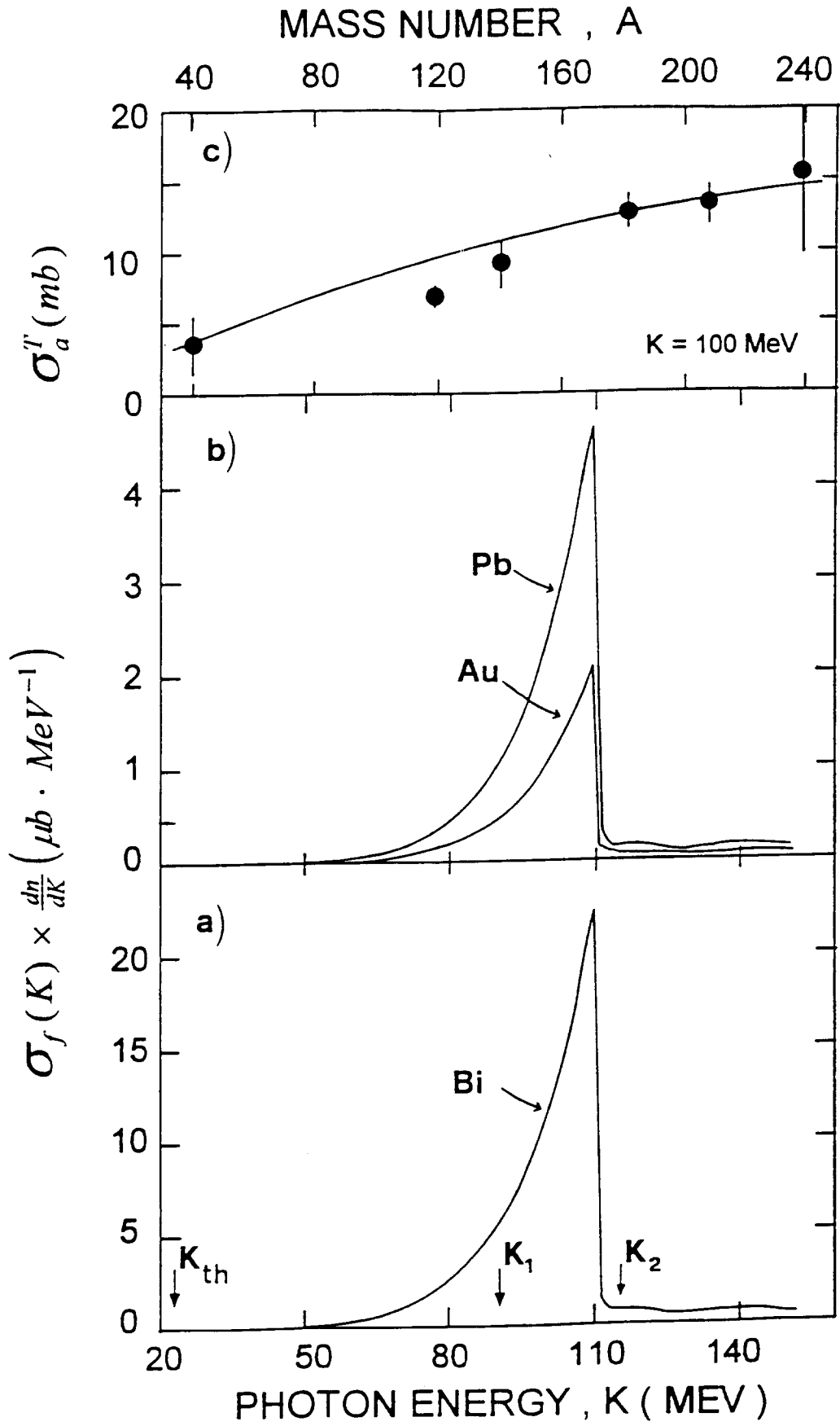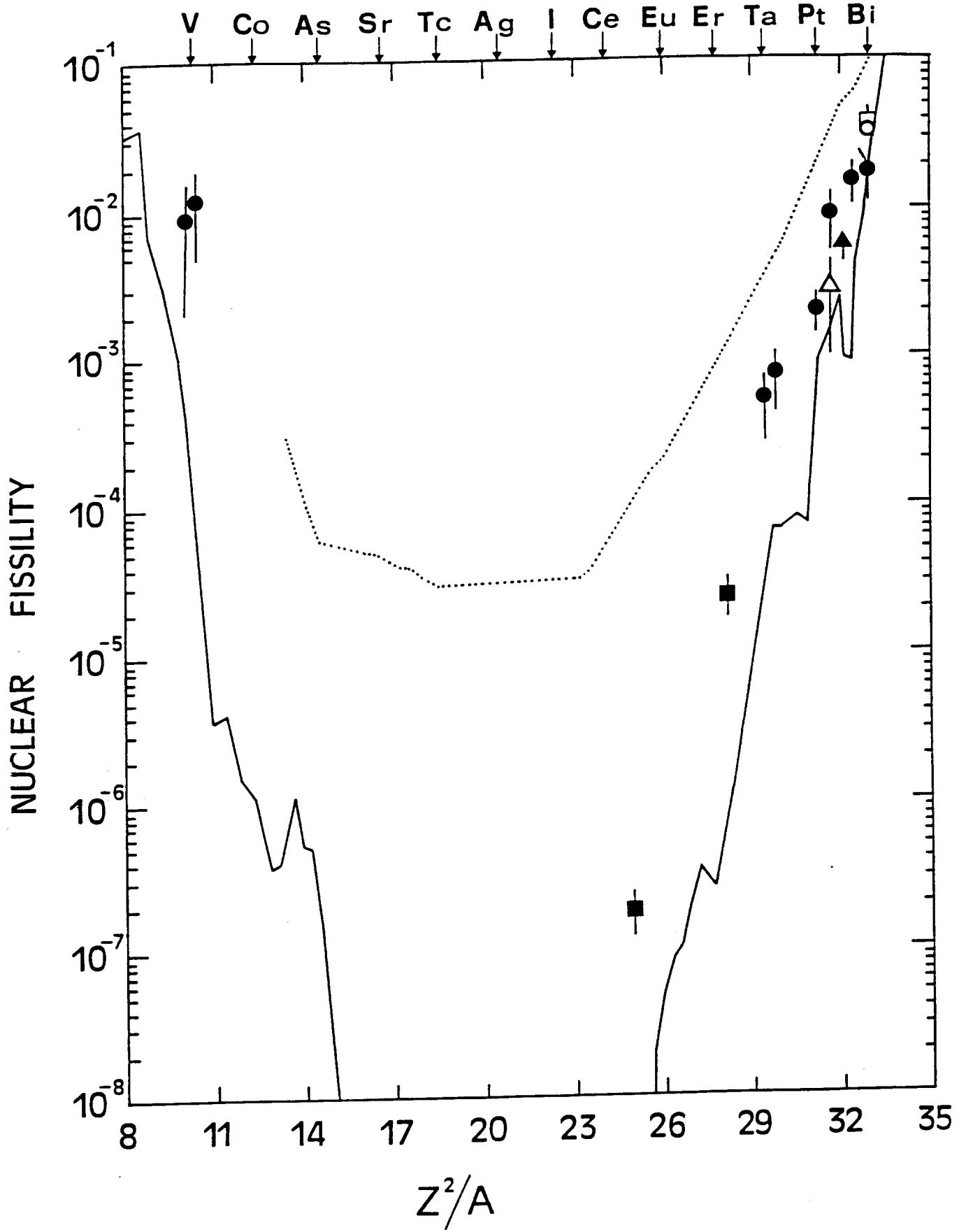
Fig. 1

Fig. 2

Fig. 3

Fig. 4

Table 1 – Data regarding the target and detector materials, exposures, etching procedure, and detector analysis of the present photofission experiment.

Target element	Target material[a]	Irradiation conditions[c]				Etching conditions	Total detector area scanned[f] (cm²)
		First run		Second run			
		Nr. of detectors[d] n_1	Nominal, total photon dose[e] Q_1 $(10^8\,\gamma)$	Nr. of detectors[d] n_2	Nominal, total photon dose[e] Q_2 $(10^8\,\gamma)$		
Bi	8 films of average thickness (5.2 ± 1.0) μm each[b]	8	3.4	8	23.0	6.25-N NaOH, 60 °C 1-h etching, gentle stirring	144
Pb	8 films of average thickness (3.1 ± 0.4) μm each[b]	8	3.4	8	23.1	idem	144
Au	8 films of average thickness (0.70 ± 0.12) μm each[b]	4	3.4	8	23.2	idem	108
Pt	20 metallic foils of 2.5 cm x 2.5 cm 26-μm thick each	20	3.4	38	23.3	idem	238
W	25 metallic foils of 2.5 cm x 2.5 cm 50-μm thick each	25	3.8	50	25.8	idem	313
Ta	24 metallic foils of 2.5 cm x 2.0 cm, 26-μm thick each, plus 6 metallic foils of 2.5 cm x 2.5 cm, 50-μm thick each	30	4.8	60	32.2	idem	375
V	6 metallic foils of 3.0 cm x 2.5 cm 15-μm thick each	6	5.5	12	37.3	6.25-N NaOH, 60 °C 1.5-h etching, gentle stirring	75
Ti	7 metallic foils of 3.0 cm x 3.0 cm, 24-μm thick each	7	5.5	14	37.5	idem	88

a) All target materials of natural isotopic composition.

b) These are high-purity metal films prepared by vacuum evaporation on 3.5 cm x 3.5 cm thin foils of Mylar (1.72 mg/cm² thick) as supports.

c) In both runs, i) Compton-edge: 109 MeV; ii) effective photon mean energy: 100 MeV; iii) photon beam intensity: 10^4 - 10^5 γ/s; iv) beam spot size at the stacks: ~1 cm x 1 cm.

d) These are sheets of 100-μm thick polycarbonate fission-track detector Makrofol N (Auftrag 90002, 0.7 Kg) supplied by Bayer AG (Germany); detectors have been placed in intimate contact with target materials forming a stack.

e) Attenuation of the photon dose throughout the sample stack estimated by the law of exponential decrease of photon beam intensity.

f) Leitz Ortholux microscopes (objectives 25x or 45x, and ocular 12.5x or 10x).

Table 2 - Data regarding the determination of photofission yield[a]

Target nucleus	C ($10^{-11}\,\mu m^3$)	Effective thickness of the target material (μm)		Detection efficiency (%)		Fission tracks recorded			Photofission yield[c] Y (mb)
		x_1	x_2	ε_1	ε_2	N_{f_1}	N_{f_2}	ΣN_f[b]	
Bi	3.56	4.0	3.8	85	87	4	22	33 ± 7	0.17 ± 0.05
Pb	3.03	3.3	3.1	69	72	3	16	24 ± 5	0.15 ± 0.04
Au	1.69	0.7	0.7	94	93	-	6	7 ± 3	$(9 \pm 4) \times 10^{-2}$
Pt	1.51	3.0	3.0	53	48	-	14	18 ± 5	$(1.9 \pm 0.6) \times 10^{-2}$
W	1.58	3.0	3.1	51	47	-	7	9 ± 4	$(7 \pm 3) \times 10^{-3}$
Ta	1.80	3.4	3.5	51	47	-	7	9 ± 4	$(4.7 \pm 2.2) \times 10^{-3}$
V	1.38	2.4	2.5	29	18	-	5	6 ± 3	$(4 \pm 2) \times 10^{-2}$
Ti	1.75	2.9	3.1	26	15	-	4	5 ± 3	$(3 \pm 2) \times 10^{-2}$

a) This is given by eq. (1); subscripts for the different quantities correspond to first and second runs.

b) Corrected for a counting efficiency of 0.79 ± 0.07; statistical error indicated.

c) Statistical plus systematic errors included.

Table 3 - Photofission and nuclear photoabsorption cross section data and fissility at 100 MeV for pre actinide and intermediate-mass nulei.

Target nucleus[a]	Z^2/A	Total nuclear photoabsorption cross section σ_a^T (mb)	Photofission cross section σ_f (mb)	Ref.	Nuclear fissility $f = \sigma_f/\sigma_a^T$
^{209}Bi	32.96	13.7 ± 1.8	0.23 ± 0.04[b]	[3]	$(1.7 \pm 0.4) \times 10^{-2}$
			0.15	[2]	$(1.1 \pm 0.1) \times 10^{-2}$
			0.35 ± 0.02[b]	[8]	$(2.5 \pm 0.4) \times 10^{-2}$
			0.48 ± 0.07	[9]	$(3.5 \pm 0.7) \times 10^{-2}$
			0.44 ± 0.07	[22]	$(3.2 \pm 0.7) \times 10^{-2}$
			0.49 ± 0.12	[21]	$(3.6 \pm 1.0) \times 10^{-2}$
			0.17 ± 0.04	[4]	$(1.2 \pm 0.3) \times 10^{-2}$
			0.21 ± 0.04[c]	[5]	$(1.5 \pm 0.3) \times 10^{-2}$
			0.24 ± 0.07	This work	$(1.8 \pm 0.6) \times 10^{-2}$
$^{207.2}$Pb	32.45	13.6 ± 1.8	0.074 ± 0.014	[4]	$(0.54 \pm 0.12) \times 10^{-2}$
			0.10 ± 0.05[c]	[5]	$(0.73 \pm 0.38) \times 10^{-2}$
			0.21 ± 0.05	This work	$(1.5 \pm 0.4) \times 10^{-2}$
^{208}Pb	32.33	13.6 ± 1.8	$(0.92 \pm 0.14) \times 10^{-1}$	[10]	$(6.8 \pm 1.4) \times 10^{-3}$
			$(0.95 \pm 0.07) \times 10^{-1}$[b]	[8]	$(7.0 \pm 1.1) \times 10^{-3}$
$^{204.4}$Tl	32.10	13.5 ± 1.8	$(7.5 \pm 2.1) \times 10^{-2}$[b]	[3]	$(5.5 \pm 1.7) \times 10^{-3}$
			$(7.6 \pm 1.5) \times 10^{-2}$[c]	[5]	$(5.6 \pm 1.3) \times 10^{-3}$
^{197}Au	31.68	13.3 ± 1.7	$(3.7 \pm 0.6) \times 10^{-2}$	[4]	$(2.8 \pm 0.6) \times 10^{-3}$
			$(3.4 \pm 2.3) \times 10^{-2}$	[23]	$(2.6 \pm 1.7) \times 10^{-3}$
			$(1.3 \pm 0.2) \times 10^{-1}$	[11]	$(9.8 \pm 2.0) \times 10^{-3}$
			$(5 \pm 1) \times 10^{-2}$[c]	[5]	$(3.8 \pm 0.9) \times 10^{-3}$
			$(1.2 \pm 0.5) \times 10^{-1}$	This work	$(9.0 \pm 3.9) \times 10^{-3}$
$^{195.1}$Pt	31.18	13.2 ± 1.7	$(1.1 \pm 0.3) \times 10^{-2}$[c]	[5]	$(0.83 \pm 0.25) \times 10^{-3}$
			$(2.6 \pm 0.8) \times 10^{-2}$	This work	$(2.0 \pm 0.6) \times 10^{-3}$
$^{183.9}$W	29.78	12.7 ± 1.7	$(9.7 \pm 4.2) \times 10^{-3}$	This work	$(7.6 \pm 3.4) \times 10^{-4}$
^{181}Ta	29.44	12.6 ± 1.6	$(3.8 \pm 0.9) \times 10^{-3}$	[11]	$(3.0 \pm 0.7) \times 10^{-4}$
			$(6.5 \pm 3.1) \times 10^{-3}$	This work	$(5.2 \pm 2.5) \times 10^{-4}$
^{174}Yb	28.16	12.3 ± 1.6	$(3.0 \pm 0.8) \times 10^{-4}$[b]	[8]	$(2.4 \pm 0.7) \times 10^{-5}$
^{154}Sm	24.96	11.3 ± 1.9	$(2.0 \pm 0.5) \times 10^{-6}$[b]	[8]	$(1.8 \pm 0.5) \times 10^{-7}$
^{51}V	10.37	4.6 ± 1.4	$(5.6 \pm 2.8) \times 10^{-2}$	This work	$(1.2 \pm 0.7) \times 10^{-2}$
$^{47.9}$Ti	10.10	4.4 ± 1.3	$(4.2 \pm 2.8) \times 10^{-2}$	This work	$(0.9 \pm 0.7) \times 10^{-2}$

[a] Mean mass number of the naturally occurring isotopes.

[b] Interpolated value.

[c] Deduced value from the measured photofission yields.

References

[1] Bernardini G, Reitz R, Segre' E 1953 Phys.Rev. 90 573

[2] Jungerman J A and Steiner H M 1957 Phys.Rev. 106 585

[3] Minarik E V and Novikov V A 1957 Sov. Phys. JETP 5 253

[4] Ranyuk Yu N and Sorokin P V 1967 Yad.Fiz.5 37 (1967 Sov.J. Nucl.Phys 5 26)

[5] Mitrofanova A V, Ranyuk Yu N and Sorokin P V 1967 Yad.Fiz. 6 703 (1968 Sov.J.Nucl.Phys. 6 512)

[6] Warnock R V and Jensen R C 1968 J.inorg.nucl.Chem. 30 2011

[7] Bellini V, Emma V, Lo Nigro S, Milone C, Pappalardo G S and Bologna G 1980 Nuovo Cimento A55 182

[8] Moretto L G, Gatti R C, Thompson S G, Routti J T, Heisenberg J H, Middleman L M, Yearian M R and Hofstadter R 1969 Phys.Rev. 179 1176

[9] Arruda-Neto J D T, Sugawara M, Tamae T, Ogino H, Miyase H and Abe K 1986 Phys.Rev C 34 935

[10] Arruda-Neto J D T, Sugawara M, Miyase H, Kobayashi T, Tamae T, Abe K, Nomura M, Matsuyama H, Kawahara H, Namai K, Yoneama M L   and Simionatto S 1990   Phys.Rev. C 41 354

[11] Arruda-Neto J D T, Saito T, Sugawara M, Tamae T, Miyase H, Abe K, Takahisa K, Konno O, Oikawa M and Simionatto S 1993   Phys.Rev. C 48 1594

[12] Leprêtre A, Beil H, Bergère R, Carlos P., Fagot J, De Miniac A and Veyssière A 1981Nucl.Phys.A 367 237

[13] Veyssière A, Beil H, Bergère R, Carlos P, Fagot J,Leprêtre A and Ahrens J 1979 Nucl.Instr.Meth. 165 417

[14] Nedorezov V G 1983 Proc. Fourth Course Int. School of Intermediate Energy Nuclear Physics (San Miniato) ed Bergère R, Costa S and Schaerf C   (World Scientific, Singapore) 434

[15] De Pascale M P, Giordano G, Matone G, Picozza P, Babusci D, Bernabei R, Casano L, D'Angelo S, Mattioli M, Prosperi D, Schaerf C, Frullani S and Girolami B 1983 Proc. Fourth Course Int. School of Intermediate Energy Nuclear Physics (San Miniato) ed   Bergère R, Costa S and Schaerf C (World Scientific, Singapore) 412

[16] Capitani G P, De Sanctis E, Guaraldo C ,Di Giacomo P, Lucherini V, Polli E, Reolon A R, Scrimaglio R, Anghinolfi M, Corvisiero P, Ricco G, Sanzone M and Zucchiatti A 1983 Nucl.Instr.Meth. 216 307

[17] Sandorfi A M, Levine M J, Thorn C E, Giordano G, Matone G and Schaerf C 1983 IEEE Trans. Nucl.Sci.NS-30 3083

[18] Kezerashvili GYa, Milov A M, and Wojtsekhowski B B 1993 Nucl.Instr.Meth. A328 506

[19] Ivanov D I, Kezerashvili G Ya, Nedorezov V G and Sudov A S 1990

Proc.of the Int. Symp.on Nucl.Phys.(Kiev) 498 ; Ivanov D I ,
Kezerashvili G Ya, Muratov V V, Nedorezov V G and Sudov AS 1991
Institute of Nuclear Research (Moscow)   preprint INR P-687 27; Ivanov
D I , Kezerashvili G Ya, Nedorezov V G , Sudov AS , Muratov V V and
Zapevalov V A 1991 Institute of Nuclear Research (Moscow) preprint
INR   P-686 26

[20] Lemke H -D, Ziegler B, Mutterer M, Theobald J P and Cârjan N 1980
       Nucl.Phys. A 342 37

[21] Bellini V, Emma V, Lo Nigro S, Milone C, Pappalardo G S, De Sanctis E,
       Di Giacomo P, Guaraldo C, Lucherini V, Polli E and Reolon A R   1983
       Nuovo Cimento Lett. 36 587

[22] Guaraldo C, Lucherini V, De Sanctis E, Levi Sandri P, Polli   E, Reolon A
       R, Lo Nigro S, Aiello S, Bellini V, Emma V, Milone C   and Pappalardo G
       S 1987 Phys.Rev C 36 1027

[23] Lucherini V, Guaraldo C, De Sanctis E, Levi Sandri P, Polli   E, Reolon A
       R, Iljinov A S, Lo Nigro S, Aiello S, Bellini V, Emma V, Milone C,
       Pappalardo G S and Mebel M V 1989 Phys.Rev.C 39   911

[24] Martins J B, Moreira E L, Tavares O A P, Vieira J L, Pinheiro Filho J D,
       Bernabei R, D'Angelo S, De Pascale M P, Schaerf C and Girolami B
       1989   Nuovo Cimento A 101 789

[25] Martins J B, Moreira E L, Tavares O A P, Vieira J L, Casano   L, D'Angelo
       A, Schaerf C, Terranova M L, Babusci D and Girolami B 1991   Phys.Rev.
       C 44 354

[26] Tavares O A P, Martins J B, de Paiva E, Moreira E L, Vieira J L,
       Terranova   M L, Capogni M, Casano L, D'Angelo A, Moricciani D, Ghio F,
       Girolami B and Babusci D   1993   J.Phys. G : Nucl.Part.Phys. 19 805

[27] Tavares O A P, Martins J B, Moreira E L, Terranova M L, Capogni M,
       Casano L, D'Angelo A, Moricciani D, Schaerf C, Girolami B, Ghio F and
       Babusci D 1993   J.Phys. G : Nucl.Part. Phys. 19 2145

[28] Tavares O A P 1991   Radiat. Effects Defects Solids 118 105

[29] Kezerashvili G Ya, Milov A, Muchnoi N Yu and Usov A 1993 Proc.
       PANIC   XIII (Perugia) vol.II 839 ; Kezerashvili G Ya, Milov A, Muchnoi
       N Yu and   Usov A 1993 Proc.Int. Symp. on Charged ParticleAccelerator
       Physics   (Dubna) vol. I 416 ; Kezerashvili G Ya, Milov A, Muchnoi N
       Yu , Dubrovin A N, Kiselev V A, Naumenkov A I, Skrinsky AN, Shatilov DN,
       Simonov E A, Petrov V V and Protopopov I Ya 1995 , High Energy
       Spin Physics, Proc. XI International Symposium (Bloomington) ed
       Heller K J   and Smith S L , AIP Press (Woodbury, N.Y.) vol. 343 260

[30] Aulchenko V M , Baibusinov B O, Baru S E, Bondar A E, Chilingarov A G,
       Filimonov G S, Kezerashvili G.Ya, Kolachev G M, Milov A M, Muchnoj N
       Yu, Purlatz T A, Romanov L V, Root N I, Shwartz B A, Sidorov V A, Titov V
       M, Zhilich V N and Zholentz A A 1995 Nucl. Instr.Meth. A355 , 261

[31] Tavares O A P and Terranova M L   1992 Nuovo Cimento A $\underline{105}$ 723

[32] Audi G and Wapstra A H   1993   Nucl.Phys. A $\underline{565}$ 1

[33] Levinger J S 1979   Phys.Lett.$\underline{82B}$ 181

[34] Rossi P, De Sanctis E, Levi Sandri P, Bianchi N, Guaraldo C,   Lucherini
     V, Muccifora V, Polli E,   Reolon A R and Urciuoli G M 1989   Phys.Rev.
     C $\underline{40}$ 2412

[35] Tavares O A P and Terranova M L 1992 J.Phys.G : Nucl.Part. Phys.$\underline{18}$
     521

[36] Terranova M L, de Lima D A and Pinheiro Filho J D   1989   Europhys.Lett.
     $\underline{9}$ 523

[37] Ahrens J, Borchert H, Czock K H, Eppler H B, Gimm H, Gundrum H,
     Kröning M, Riehn P, Sita Ram G, Zieger A and Ziegler B   1975
     Nucl.Phys.   A $\underline{251}$ 479

[38] Nix J R and Sassi E   1966   Nucl.Phys. $\underline{81}$ 61

[39] Iljinov A S, Cherepanov E A and   Chigrinov S E   1980 Yad.Fiz. $\underline{32}$ 322
     (1980 Sov. J.Nucl.Phys. $\underline{32}$ 166)

NOTAS DE FÍSICA é uma pré-publicação de trabalho original em Física.
Pedidos de cópias desta publicação devem ser enviados aos autores ou ao:

NOTAS DE FÍSICA is a preprint of original unpublished works in Physics.
Requests for copies of these reports should be addressed to: